Spacecraft Contamination from Scarfed Nozzle Exhausts

S. Boraas*
Morton Thiokol, Inc., Brigham City, Utah

A rocket operating in a vacuum environment will produce a molecular flow that is directed into the nozzle backflow region. This paper discusses the development and application of an analytical model which describes this flow and provides a means of predicting the exhaust plume contamination from a scarfed nozzle. The model is an adaptation of one previously developed for a conventional unscarfed nozzle. It is based upon the existence of a small, conical-shaped continuum region downstream of the nozzle exit from which the directed flow originates as a result of molecular effusion. The model was programmed on the computer and provides a quick and convenient means of estimating the maximum contamination. Results using the earlier model for conventional nozzles compared favorably with limited test data; however, no known contamination data for scarfed nozzles are available for a comparison with this model's predictions. When used to predict contamination from the Peacekeeper missile attitude control engine (ACE) and the Star 30 space motor, the model indicated that scarfing will dramatically increase the contamination of surfaces in the backflow region.

Nomenclature

A = coefficient in Maxwell's equation
a = axial coordinate of point P in backflow region (Fig. 3)
b = radial coordinate of point P in backflow region (Fig. 3)
$\bar{d}$ = distance between point P and cone surface (Fig. 3)
E = energy
$\dot{e}$ = energy flow rate or energy flux at point P
F = view factor
f = fraction of all molecules that will impinge at point P
$f(\theta)$ = mass function
K_M = mass exponent
L = length
M = Mach number
m = molecular mass
$\dot{m}$ = mass flow rate or mass flux at point P
n = molecular density
$\bar{N},\bar{n}$ = normal vectors (Fig. 3)
P,p = total pressure, static pressure
r = nozzle or cone radius
$\bar{r}$ = distance between point P and origin (Fig. 3)
R = specific gas constant, ratio
S = contributing cone surface area
T = temperature
U = mass flow velocity
u = atomic mass unit (1.66×10^{-27} kg)
v = thermal velocity
W = molecular weight
x,y,z = Cartesian coordinates
α = angle (Fig. 3)
α_p = plume centerline displacement angle (Fig. 7)
β = exponent in Maxwell's equation, angle (Fig. 3)
β_s = scarf angle
γ = specific heat ratio
δ = boundary layer thickness, cone semivertex angle
ϵ = nozzle area ratio, angle (Fig. 4)
μ,ν,τ,ϕ,ψ = angles (Fig. 3)
η = angle (Fig. 4)
θ = wall angle, angular distance of point P (Figs. 1, 3)
λ = Hill-Draper plume shape parameter
ρ = density
χ = meridional angle of point P (Fig. 2)
$d\sigma$ = incremental surface at point P
$d\omega$ = incremental solid angle

Subscripts

av = average
b = boundary layer, cone base
c = scarf plane/nozzle centerline intersection station (Fig. 2)
d = data match
e = nozzle exit
i = impinging, incident
ℓ = lower
min = minimum
max = maximum
n = nozzle, nozzle wall
P = point P
r = reflected
s = scarf station (Fig. 2)
t = throat
0 = stagnation

Introduction

THE problem of backflow contamination was recognized in the early days of the space program.[1] At that time, questions were being raised concerning the related problem of backflow heating of the spacesuit to be worn by a lunar explorer equipped with a backpack maneuvering unit. The concern in recent years stems from the fact that this backflow will almost certainly contaminate and degrade the performance of antennas, solar cells, thermal blankets, etc., located in the backflow region. The difficulty of predicting this flow has led to several experimental studies[2-4] to determine its magnitude.

Analytically, the prediction of the backflow is hampered by the noncontinuum nature of the inviscid plume at large angular distances from the nozzle axis. It is further complicated by the acceleration of the nozzle wall boundary layer upstream of the nozzle lip and its expansion into the backflow region.[5] These problems have been treated using the Monte

Received July 25, 1986; revision received Dec. 5, 1986.

*Supervisor, Aero/Thermal Section, Motor Performance Department, Space Operations. Member AIAA.

Carlo method to characterize the flowfield in the nozzle lip region[6] but this technique, although presumably satisfactory, requires an enormous amount of computer time.

Reference 7 describes a previously developed simple, uncomplicated model for calculating the contamination potential at a point in the backflow region of a conventional nozzle and does so in about 0.25 s on an IBM 370 computer. This model was based upon the concept that an analytically derived, conical-shaped, inviscid gas continuum region exists immediately downstream of the nozzle exit. The molecular flow into the backflow region originates at the cone's surface and is a result of a molecular effusion based upon a superposition of the Maxwellian distribution of the exhaust gas thermal velocities and the gas flow velocity. The model incorporates the effect of the expanding boundary layer by either expressing the inviscid cone surface gas properties in terms of a specified Mach number that is a fraction of the inviscid flow Mach number in the nozzle at the cone base station or as an equivalent surface Mach number resulting from a partial "blanketing" of the surface by the boundary layer.

The difficulties associated with predicting the backflow from a conventional nozzle become increasingly so when the nozzle is scarfed. In a nonvacuum environment, where the entire plume can be treated as a continuum, either an approximate description[8] of it or an exact characteristic solution[9] are possible. In a recent study, Romine and Noble[10] developed a model of the three-dimensional vacuum plume from a scarfed nozzle, but restricted the expansion to the region downstream of the limiting continuum streamlines emanating from all points on the nozzle lip periphery. Since, by definition, the backflow region is upstream of the limiting streamline, this vacuum plume solution is clearly inadequate for describing the backflow. From these considerations, and the fact that the previously developed contamination model for conventional nozzles had already proved successful, the logical approach to the development of a model for scarfed nozzles appeared to be modification of the earlier model. This was done by defining an "equivalent" conical continuum region when the nozzle is scarfed and providing a means of accounting for the nonsymmetry of the flow into the backflow region. Several other changes and improvements were also incorporated, the result was a more versatile model capable of predicting the backflow contamination from both scarfed and unscarfed nozzles.

The developed model was used to predict the contamination from the plume of the Peacekeeper post boost vehicle (PBV) attitude control engine (ACE), which has a highly scarfed nozzle. The model was also used to determine the effect that scarfing would have on the back flow contamination from the Star 30 high-performance kick motor if its nozzle was scarfed. The predictions for the ACE and the Star 30 motor indicated that scarfing will increase surface contamination in the backflow region. In particular, increasing scarfing increases the contamination unless the surface in question lies in a plane normal to the scarf plane and contains the minor axis of the elliptical scarf plane/nozzle intersection. No known contamination data are available to verify these or any other scarfed nozzle predictions.

A description of the model development, the calculations made, and the conclusions reached during this study are given in the subsequent sections.

Model Development

The new model was developed with the intent of retaining most of the features of the original model, while making it adaptable to determining the contamination potential of both scarfed and unscarfed nozzles. Contamination potential or maximum potential is defined as the total molecular flow impinging on a surface in the backflow region, recognizing that not all impinging molecules will necessarily adhere and have a contaminating or adverse influence.

In the development of this new model, some improvements and additions were incorporated, the most notable being the specification of the actual nozzle contour and the scarf plane location. The primary task was the definition of an equivalent conical continuum region downstream of the nozzle exit plane when the nozzle is scarfed. Having determined this, the portion of the conical surface contributing to the flow into the backflow region was defined in the same manner as before. Coupled with previously derived mass and heat backflow equations, which remain unchanged, a new model was obtained for predicting the contamination potential and the associated heating of a surface in the backflow region. A brief description of the development of this model, including the definition of the equivalent continuum region and its contributing surface and a listing of the primary equations, are given in the following paragraphs.

Continuum Region

It has been postulated[1,11] that, when a conventional nozzle is exhausting into a vacuum and if the flow at the nozzle exit is a continuum, then the continuum column of exhaust gases emerging from the nozzle exit will erode as a consequence of molecular effusion at the column boundaries to become a cone whose semivertex angle is

$$\delta = \tan^{-1}\left[\left(\frac{1}{2M_e \cos\theta_e}\right)\left(\frac{2}{\gamma\pi}\right)^{1/2}\right] \qquad (1)$$

where M_e and θ_e are the inviscid Mach number and wall angle at the nozzle exit and γ is the gas specific heat ratio. A schematic of this continuum cone is shown in Fig. 1a for a conventional nozzle as it relates to the molecular flow impinging at point P in the backflow region well forward of the Prandtl-Meyer limiting streamline. Only the shaded portion

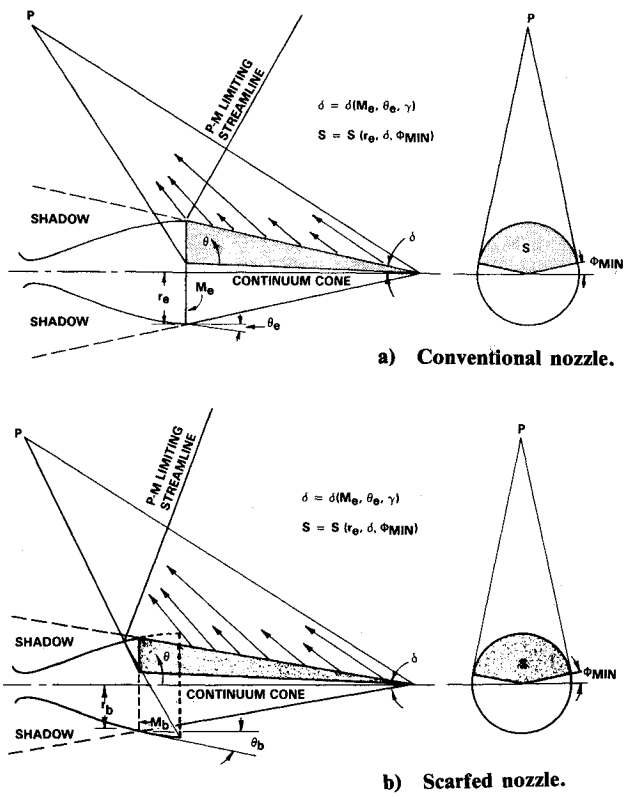

Fig. 1 Molecular effusion from continuum cone surface into the backflow region.

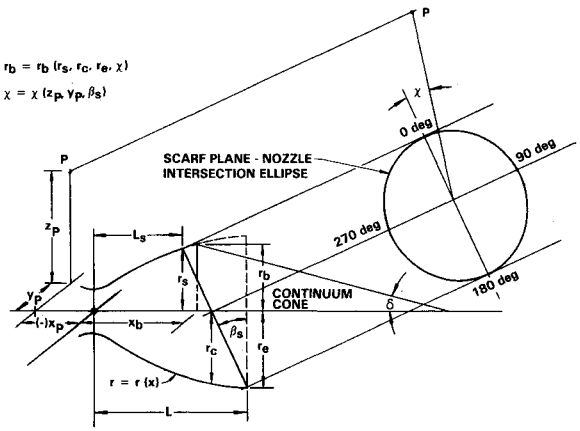

Fig. 2 Scarfed nozzle geometry.

of the cone's surface that is visible at P will actually contribute to the flux arriving there. Therefore, the axial and radial distances of point P relative to the base of the cone and the nozzle centerline, respectively, are important in determining the size of the contributing surface. However, the circumferential position of point P plays no part in this determination since the flow from the nozzle is axisymmetric. If point P lies in the shadow of the nozzle, the cone surface is invisible and there is no flow impingement.

Figure 1b shows the molecular flow impinging at the same point P when the same nozzle is scarfed. Point P is still in the backflow region, despite the fact that the limiting streamline is now located at a larger angular distance θ from the nozzle axis. It is now assumed that the equivalent continuum cone that produces the backflow to point P is a cone extending into the nozzle whose base radius is less than the unscarfed nozzle exit radius. It will be shown that the base radius of the cone is a function of the scarf plane location and the circumferential location of point P expressed as a meridional angle χ in the plane parallel to the scarf plane. This meridional angle is zero in Fig. 1.

Figure 2 shows the geometry of a scarfed nozzle and the location of point P relative to a Cartesian coordinate system whose origin is on the centerline at the nozzle throat. From the known nozzle contour and the scarf plane angle β_s or location, the nozzle radii at the intersection of the plane and the nozzle r_s and the centerline r_c are defined. These, along with the unscarfed nozzle exit radius r_e and the meridional angle of point P, permit definition of the base radius of the equivalent continuum cone. This radius is

$$r_b = \left(\frac{r_s + r_c}{2}\right)\left(1 - \frac{\chi}{90}\right) + r_c\left(\frac{\chi}{90}\right) \quad \text{for } 0 \le \chi \le 90 \tag{2a}$$

$$r_b = r_c\left[1 - \left(\frac{\chi - 90}{90}\right)\right] + \left(\frac{r_c + r_e}{2}\right)\left(\frac{\chi - 90}{90}\right)$$

$$\text{for } 90 < \chi \le 180 \tag{2b}$$

$$r_b = \left(\frac{r_c + r_e}{2}\right)\left[1 - \left(\frac{\chi - 180}{90}\right)\right] + r_c\left(\frac{\chi - 180}{90}\right)$$

$$\text{for } 180 < \chi \le 270 \tag{2c}$$

$$r_b = r_c\left[1 - \left(\frac{\chi - 270}{90}\right)\right] + \left(\frac{r_s + r_c}{2}\right)\left(\frac{\chi - 270}{90}\right)$$

$$\text{for } 270 < \chi \le 360 \tag{2d}$$

In Eq. (2), the meridional angle is expressed as follows in terms of the coordinates of point P in the y-z plane and the scarf angle.

$$\chi = \tan^{-1}\left(\frac{y_P}{z_P \cos\beta_s}\right) \quad \text{for } z_P > 0,\ y_P \ge 0 \tag{3a}$$

$$\chi = 360 + \tan^{-1}\left(\frac{y_P}{z_P \cos\beta_s}\right) \quad \text{for } z_P > 0,\ y_P < 0 \tag{3b}$$

$$\chi = 180 + \tan^{-1}\left(\frac{y_P}{z_P \cos\beta_s}\right) \quad \text{for } z_P < 0, \text{ all } y_P \tag{3c}$$

$$\chi = 90 \text{ for } z_P = 0,\ y_P > 0 \tag{3d}$$

$$\chi = 270 \text{ for } z_P = 0,\ y_P \le 0 \tag{3e}$$

The one-dimensional Mach number M_b at the base of the equivalent cone will be less than that at the unscarfed nozzle exit and the nozzle wall angle θ_b at the cone base will be greater. This means that the semivertex angle of the equivalent cone as calculated from Eq. (1) will be greater than that of the unscarfed nozzle cone. Together with its smaller base, this results in its total surface being less. Although its total surface area is less, the potential for contamination from the equivalent cone will be greater due to increased thermal energy and the reduced kinetic energy of the gas comprising it.

Contributing Surface

As shown in Fig. 1, only that part of the cone's surface visible at point P will actually contribute to the flux arriving there. Therefore, the location of a point relative to the cone is important in determining the portion of the cone surface that contributes to the contamination at the point. This was determined previously[7,11,12] using the continuum cone/point P schematic of Fig. 3. In this geometrical representation, the origin of the Cartesian coordinate system was chosen to be on the nozzle centerline at the base of the cone, with the cone height being colinear with the positive x axis. An incremental surface $d\sigma$ located at point P $(-a,b)$ is oriented such that the angle between it and a plane perpendicular to the nozzle centerline is ψ. The vectoral distance between point P and a point x,r on the cone surface is $\bar{d}$ and α and β are the angles between the x axis and the projection of $\bar{d}$ on the vertical and horizontal planes, respectively. Similarly, $\bar{r}$ is the radius vector between point P and the origin. The angle between the vectors $\bar{d}$ and $\bar{n}$ is μ and the angle between vectors $\bar{r}$ and $\bar{n}$ is ν. The angle between $\bar{d}$ and the outward pointing normal vector $\bar{N}$ at the cone surface is θ and ϕ is the meridian angle in the plane containing the cone base, as shown in Fig. 1.

The contributing surface of the cone is that portion of the total surface for which angle τ is equal to or less than $\pi/2$. When $\tau = \pi/2$, a minimum value of ϕ is defined, which along with the known semivertex angle and the cone base radius

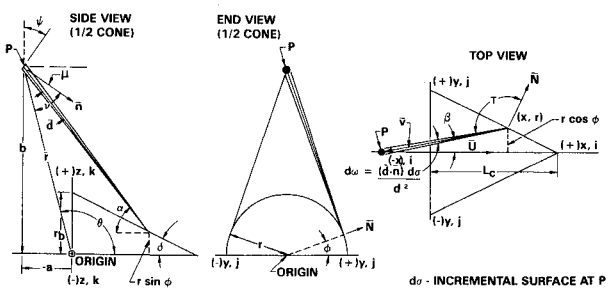

Fig. 3 Continuum cone geometry.

permits the calculation of the contributing surface area as

$$S=\left(\frac{\pi r_b^2}{2\sin\delta}\right)\left(\frac{\pi-2\phi_{\min}}{\pi}\right) \tag{4}$$

where $r_b=r_e$ for a conventional nozzle and is the value obtained from Eq. (2) for a scarfed nozzle.

Mass and Heat Flow Equations

The molecular velocity distribution of the gas on the cone surface may be represented by the Maxwellian distribution of thermal velocities for a stationary gas, since the thermal velocity distribution is unaffected by its mass motion. This distribution is the basis for determining the convective mass and heat flow equations for the molecular flow directed into the backflow region. Developed earlier, they are repeated here.

Mass Flow Equation

Consider the molecular effusion directed toward point P from a unit area of the cone's contributing surface as shown in Fig. 4. The molecular flux on the incremental surface $d\sigma$ at P is

$$dN=nAF\cdot d\sigma\cdot\cos(\tau+\epsilon)\int_{-v_\ell}^{-\infty} v^3e^{-\beta^2v^2}dv \tag{5}$$

where n is the molecular density of the continuum cone. A and β the coefficient and exponent in the distribution function and F is the view factor. For finite values of both the thermal v and mass velocities U, a molecule must depart from the cone surface with a thermal velocity equal to or greater than some minimum velocity and at an angle $(\eta+\epsilon)$ relative to the mass velocity direction if it is to reach point P. This minimum velocity, which is $U\cos(\eta+\epsilon)$, becomes the lower limit on the thermal velocity in Eq. (5). Integrating Eq. (5), multiplying by the area of the contributing surface, and replacing the molecular density with the gas density ρ, the total mass flow rate impinging on the surface $d\sigma$ at point P becomes

$$d\dot{m}=\frac{\rho AF\cdot[\beta^2(UC)^2+1]\cdot d\sigma S}{2\beta^4e^{\beta^2(UC)^2}} \tag{6}$$

where $C=\cos(\eta+\epsilon)$ and where the modified view factor becomes

$$F=\frac{\cos\beta(\cos\alpha\cos\psi+\sin\alpha\sin\psi)\cos(\tau+\epsilon)}{b^2-2b(r_e-x\tan\delta)\sin\phi+(r_e-x\tan\delta)^2+(a+x)^2} \tag{7}$$

The fraction of all molecules having thermal velocities between the lower and upper limits of Eq. (5) and capable of impinging at point P is

$$f=1+\left(\frac{2}{\pi^{1/2}}\right)xe^{-x^2}-\left(\frac{2}{\pi^{1/2}}\right)\int_0^x e^{-x^2}dx \tag{8}$$

where $x=\beta v$. The average thermal velocity of the impinging molecules is

$$v_{\text{av}}=\left(\frac{2}{\pi^{1/2}}\right)\beta^{-1}(x^2+1)e^{-x^2}f^{-1} \tag{9}$$

and the molecular density of the flow impinging at point P is

$$n_i=\frac{d\dot{m}}{v_{\text{av}}\cdot W\cdot u} \tag{10}$$

For comparison with test data, the mass flow rate of Eq. (6) is expressed in terms of flow rate per unit solid angle $d\omega$ subtended by surface $d\sigma$ at the origin as

$$\left(\frac{d\dot{m}}{d\omega}\right)_\theta=\frac{d\dot{m}\cdot r^2}{\sin\theta\sin\psi-\cos\theta\cos\psi} \tag{11}$$

Nondimensionalizing this by its equivalent value along the positive x axis ($\theta=0$), which is

$$\left(\frac{d\dot{m}}{d\omega}\right)_{\theta=0}=\frac{\dot{m}_n\lambda}{\pi^{3/2}} \tag{12}$$

as given by Chirivella[2] using the plume shape parameter λ defined by Hill and Draper[13] gives the mass flow rate as a function of the angular position. This function can then be expressed in terms of a θ dependent mass exponent K_M as

$$f(0)=10^{K_M} \tag{13}$$

Heat Flow Equation

Each of the molecules impinging upon surface $d\sigma$ will impart to it a translation kinetic energy $mv^2/2$, where m is the mass of a single molecule. The molecular kinetic energy emanating from a unit area of the cone's contributing surface and incident upon the incremental surface at point P was determined in a manner similar to that used in deriving dN. It is

$$dE_i=nAF\cdot d\sigma\int_{-v_\ell}^{-\infty}\frac{v^3e^{-\beta^2v^2}\cdot mv^2dv}{2} \tag{14}$$

where F is the modified view factor as defined in Eq. (7). Integrating this equation, multiplying by the contributing area of the cone surface, and expressing the results in terms of the flow density gives the total incident energy as

$$dE_i=\frac{\rho AF[\beta^4(UC)^4+2\beta^2(UC)^2+2]d\sigma S}{4\beta^6e^{\beta^2(UC)^2}} \tag{15}$$

If the assumption is made that the accommodation coefficient is unity on surface $d\sigma$, then the impinging molecules at the gas temperature T will be completely accommodated and re-emitted with a Maxwellian velocity distribution that is compatible with the surface temperature T_P at point P. This reflected translation energy is

$$dE_r=\frac{\rho AF(T_P/T)[\beta^2(UC)^2+1]d\sigma S}{2\beta^6e^{\beta^2(UC)^2}} \tag{16}$$

The net transfer of kinetic energy at the surface is the incident energy less the reflected energy, which represents the net

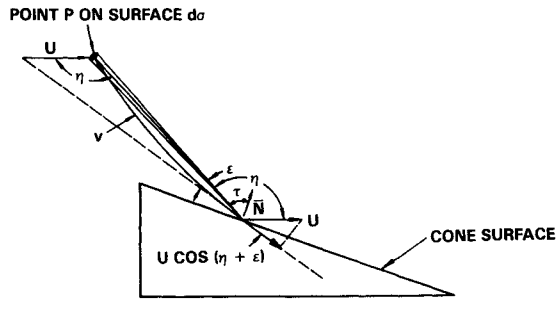

Fig. 4 Path of impinging molecules.

convective energy flow at point P for a monatomic gas. It is an approximation of the net energy flow for a diatomic gas for which energy exchanges at the surface caused by additional degrees of freedom will probably have to be considered. From Eqs. (15) and (16), the net transfer of energy is

$$d\dot{e} = \frac{\rho AFS d\sigma}{2\beta^6 e^{\beta^2(UC)^2}} \left\{ \left[\frac{\beta^4 (UC)^4 + 2\beta^2 (UC)^2 + 2}{2} \right] - \frac{T_P}{T} [\beta^2 (UC)^2 + 1] \right\} \quad (17)$$

or in terms of the cone surface properties γ, p, T, and M,

$$d\dot{e} = \frac{2pFS d\sigma (R/T)^{1/2}}{e^{(\gamma/2)(MC)^2}} \left\{ \frac{T}{4} [(MC)^4 \gamma^2 + 4(MC)^2 \gamma + 8] - T_P [(MC)^2 \gamma + 2] \right\} \quad (18)$$

Except for Eqs. (2) and (3), Eqs. (1-18) are the basic equations in the original model. The revision in this study to accept the actual nozzle contour, the scarf plane location, and a three-coordinate (x_P,y_P,z_P) description of the point P location resulted in a more versatile model. The model retains the option of calculating the contamination potential by using either a specified cone surface Mach number based on data matching or the computed equivalent value due to boundary-layer expansion. Both the original and revised models can also calculate the contamination when the surface Mach number is selected to be that in the inviscid region or in the boundary layer at the nozzle station corresponding to the cone base.

Application

A brief review of the previous application of the original model to a conventional nozzle will be made prior to discussing the results of applying the revised model to the Peacekeeper ACE and Star 30 nozzles.

Conventional Nozzles

The key finding in the application of the earlier model to a conventional nozzle was the fact that the ratio M_d/M_e of the specified cone surface Mach number M_d matching the test data to the inviscid value M_e at the nozzle exit was relatively constant for all gaseous media for which backflow data were available. The ratio was 0.62–0.75, being 0.62–0.65 for nitrogen[2,3] over a wide temperature range (529–2,340°R), 0.75 for carbon dioxide,[2] and an intermediate value of 0.71 for a liquid rocket engine burning N_2O_4/MMH.[4] This suggested that the ratio is somewhat dependent upon the exhaust gas composition, but not to a great degree. What is significantly more important is the fact that a good prediction of the contamination potential for either a conventional or scarfed nozzle can be obtained when this ratio is specified in an application of the model.

Figure 5 (obtained from Ref. 7) shows the variation of the mass exponent with angular distance for one of the nozzles used by Chirivella.[2] A cone surface Mach number M_e corresponding to the inviscid value at the nozzle exit greatly underpredicts the data (shown in the cross-hatched region), as one might expect, since boundary-layer expansion is not included. However, not too surprsingly, this Mach number gives a value of K_M that is quite close to an inviscid value computed by Grier[14] at $\theta = 90$ deg. The model developed by Grier assumed a molecular effusion into the backflow region from a continuum surface defined as the axisymmetric surface in the inviscid plume where the Knudsen number has a constant value of 1.0.

The influence of the boundary layer is very apparent in Fig. 5. If the very conservative assumption is made that the cone surface Mach number is that in the boundary layer M_b, then the model overpredicts the data. The Mach number which matches the data is an intermediate value equal to 0.62 M_e. With this value, the computed variation of K_M with θ is very similar to that obtained from the test data out to an angular distance of 160 deg. At that point, the value of K_M starts to decrease rapidly. Beyond an angular distance of 177 deg, the impingement point lies in the nozzle shadow ($K_M = -\infty$), defined as the region where the angular distance $\theta > (180 - \delta)$. Based on these results, the original model appeared capable of predicting reasonably well the variation of mass exponent with angular distance. The model also predicted what may be significant backflow into a region more than 125 deg beyond the limit predicted by continuum theory.[13]

The earlier model had also demonstrated its capability in a parametric study to determine the effect of nozzle geometry, impingement surface orientation, stagnation conditions, and gas physical properties on the magnitude of the impinging backflow. Some of these results were confirmed by existing test data where the effects of similar parameters had been investigated. For example, the results indicated that the backflow and hence the degree of contamination decreases with increasing nozzle area ratio and nozzle wall angle. Increasing chamber pressure had the effect of decreasing backflow slightly as a result of a decreased boundary-layer influence. This was in agreement with Chirivella's data.[2] For combustion gases where the ratio of specific heats is 1.25 or less, the backflow appeared quite insensitive to variations in the specific heat ratio and the molecular weight. This was consistent with the conclusion by Alt[4] that oxidizer to fuel mixture ratio had no pronounced effect on the backflow. These and the previously discussed results for conventional nozzles give credence to the belief that the more versatile model developed in this study should be able to adequately predict the contamination of scarfed nozzles for which no known contamination data exist.

Scarfed Nozzles

The model developed in this study was first used to determine the contamination from the Peacekeeper ACE nozzle. This nozzle was selected because it represents the only scarfed nozzle for which the plume has been experimentally determined at near-space conditions.[15] Consequently, it provided information on the skewness of the plume that might relate to the degree of contamination.

The ACE nozzle, which is scarfed at 46.4 deg, is shown in Fig. 6 along with portions of the 0.05 lb/ft^2 plume dynamic pressure contour obtained from tests at a simulated 400 kft altitude in Calspan's high-altitude test chamber. Calculations of the contamination potential were made for the actual scarfed configuration as well as for other scarf angles, including an unscarfed version, and the results are shown in tabular form in Fig. 6.

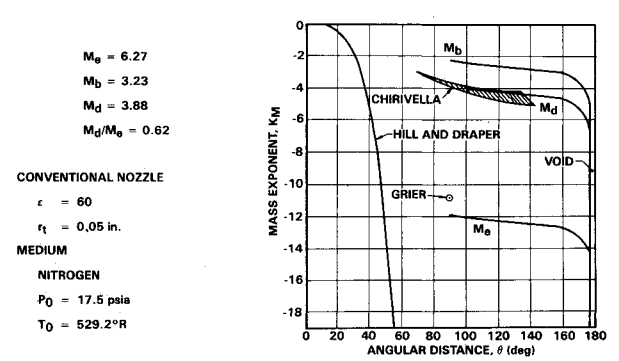

Fig. 5 Variation of mass exponent with angular distance.

Noble and Romine[16] developed a source flow model of the scarfed ACE nozzle exhaust plume. With this model, they predicted a plume centerline displacement angle α_P of 4 deg due to scarfing, as shown in Fig. 6. Using an adaptation of this model along with the plume data base, Calspan calculated the angle to be 11 deg. The values of nozzle thrust F and the plume inclination angle shown for different scarf angles in the table of Fig. 6 were computed using the scarf nozzle performance model developed by Boraas.[17] It is seen that, at the nozzle scarf angle of 46.4 deg, the plume displacement angle of 3.91 deg as computed by this model is essentially that predicted by the Noble-Romine model.

The mass flux values $\dot{m}_P$ shown in the table of Fig. 6 represent the computed contamination potential, at the arbitrarily selected point P shown, for various degrees of scarfing, including the actual scarf angle. These values were determined using an assumed cone surface Mach number ratio M_d/M_e of 0.7 based upon the previous discussion of this ratio. The ratio $R_{\dot{m}}$ of these mass flux rates to that of an unscarfed nozzle indicates that the contamination potential increases rapidly with increasing scarf angle; the increase being more than fourfold ($R_{\dot{m}}=4.16$) over the 46.4 deg scarf angle variation shown. Although possibly fortuitous, there appears to be something of a one-to-one correspondence between the increasing skewness of the plume as represented by α_P and the nondimensionalized increase in the contamination as denoted by $R_{\dot{m}}$.

Figure 7 also shows the Peacekeeper ACE nozzle and the effect of rotating the same point P of Fig. 6 around the motor centerline. The plot shows the effect of the point's circumferential location (expressed as the meridional angle) on several flow quantities expressed as a ratio R of a quantity at a given value of the meridional angle nondimensionalized by its corresponding value at $\chi=0$ deg. The quantities computed are the mass flux $\dot{m}$, energy flux $\dot{e}$, number density n_i of the impinging flow, fraction f of all molecules on the continuum cone's surface capable of reaching the point, and average velocity v_{av} of the molecules arriving there.

The results of Fig. 7 show that the contamination potential, expressed by $R_{\dot{m}}$, decreases with increasing χ until a minimum is reached at $\chi=180$ deg, beyond which it increases again in a similar manner. These results are consistent with the effects of scarf angle as shown in Fig. 6, since increasing χ from 0 to 180 deg is comparable to decreasing the scarf angle and therefore decreasing the possible contamination; increasing χ from 180 to 360 deg is comparable to increasing the scarf angle and increasing the contamination. Similar effects of χ on the energy flux and the number density are shown.

Since increasing χ from 0 to 180 deg in Fig. 7 is comparable to decreasing scarfing, the net effect is an increased gas flow velocity within the continuum cone. This means a decreased likelihood of cone surface molecules reaching point P and, therefore, a decrease in the molecular fraction.

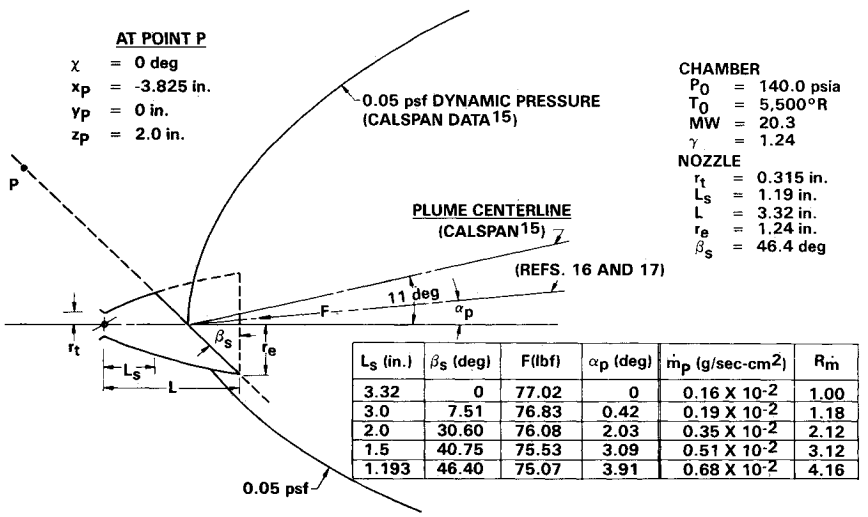

L_s (in.)	β_s (deg)	F(lbf)	α_p (deg)	$\dot{m}_P$ (g/sec-cm^2)	$R_{\dot{m}}$
3.32	0	77.02	0	0.16×10^{-2}	1.00
3.0	7.51	76.83	0.42	0.19×10^{-2}	1.18
2.0	30.60	76.08	2.03	0.35×10^{-2}	2.12
1.5	40.75	75.53	3.09	0.51×10^{-2}	3.12
1.193	46.40	75.07	3.91	0.68×10^{-2}	4.16

Fig. 6 Peacekeeper ACE nozzle: effect of scarfing on contamination potential.

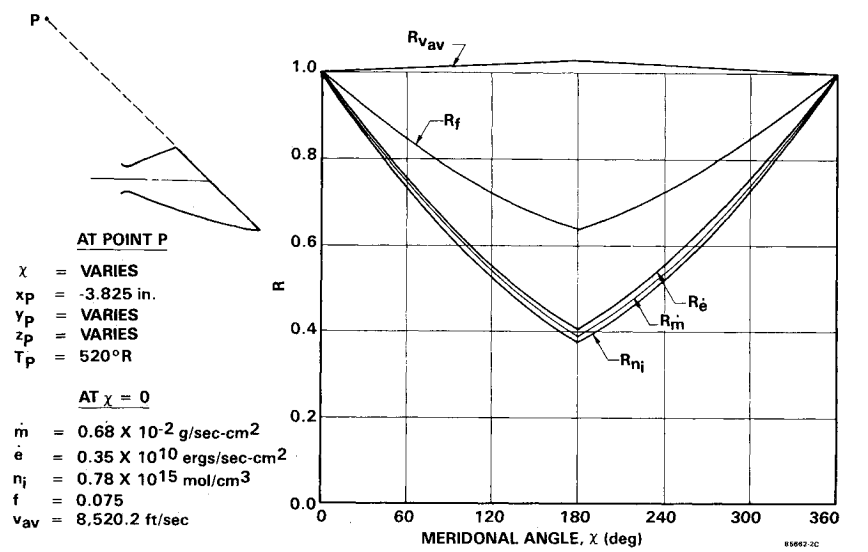

Fig. 7 Peacekeeper ACE nozzle: effect of meridional angle on backflow properties.

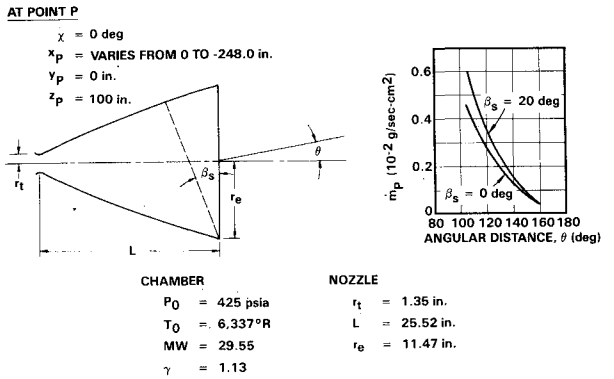

Fig. 8 Contamination from the Star 30 high-performance kick motor.

On the other hand, the increased gas flow velocity means that only surface molecules with thermal velocities exceeding the gas velocity will have the capability of reaching point P; thus, the average velocity of the impinging molecules will increase. Both these effects are shown in Fig. 7; opposite effects for each occur in the 180-360 deg region.

A second application of the model determined what effect scarfing would have on surfaces far forward of the nozzle exit of the Star 30 high-performance kick motor. The mass flux results, shown as a function of angular distance in Fig. 8, are for a series of surface points at a radial distance of 100 in. from the nozzle centerline and varying axially from the throat location to a point 248.0 in. forward of the nozzle throat. As already shown in Fig. 5, the mass flux decreases with increasing angular distance, the effect being more dramatic in Fig. 8 in which mass flux rather than mass exponent is plotted. Scarfing the nozzle increases the potential contamination, but the increase decreases with increasing angular distance. At a large angular distance such as $\theta = 160$ deg, the effect of scarfing is negligible.

Conclusions

A mathematical model has been developed for determining the backflow contamination potential from a scarfed nozzle plume in a space environment. Applied to the Peacekeeper ACE and the Star 30 motor, the following conclusions can be made concerning the results obtained:

1) Scarfing a nozzle will increase the contamination potential at a point in the backflow region relative to that of an unscarfed nozzle, unless the point lies at the 180 deg meridional location in which case there is no effect.

2) Increasing the scarfing angle increases the contamination potential unless the point lies at the 180 deg meridional location.

3) When the meridional angle of the point increases from 0 to 180 deg, the contamination potential will decrease. Increasing the angle from 180 to 360 deg will increase the potential.

4) The increase in the contamination potential due to scarfing will decrease as the angular distance of the point increases.

References

[1]Boraas, S., "Approximate Solutions to the Problem of Convective Heating of a Surface in the Vicinity of a Rocket Exhausting into Vacuum," Bell Aerospace Corp., Buffalo, NY, Rept. 7500-92001, Oct. 1963.

[2]Chirivella, J. E., "Molecular Flux Measurements in the Back-Flow Regions of a Nozzle Plume," Jet Propulsion Laboratory, California Institute of Technology, Pasadena, CA, Tech Memo 33-620, July 1973.

[3]Calia, V. S. and Brook, J. W., "Measurements of a Simulated Rocket Exhaust Plume Near the Prandtl-Meyer Limiting Angle," *Journal of Spacecraft and Rockets*, Vol. 12, April 1975, pp. 205–208.

[4]Alt, R. C., "Bipropellant Engine Plume Contamination Program," AEDC-TR-79-28, Vol. 1, Dec. 1979.

[5]Simons, G. A., "Effect of Nozzle Boundary Layers on Rocket Exhaust Plumes," *AIAA Journal*, Vol. 10, Nov. 1972, pp. 1534–1535.

[6]Chirivella, J. E., Baroth, E. C., and Guernsey, C. S., "Nozzle Lip Flow and Self-Scattering Collisions as Contributors to Plume Backflow," *JANNAF 13th Plume Technology Meeting*, CPIA Pub. 357, Vol. 1, April 1982, pp. 19–38.

[7]Boraas, S., "Spacecraft Contamination from Rocket Exhausts," AIAA Paper 81-1385, July 1981.

[8]Boraas, S. and Ashby, R. L., "Installed Thrust Vector for Scarfed Nozzles," *Journal of Spacecraft and Rockets*, Vol. 6, Dec. 1969, pp. 1410–1415.

[9]Vadyak, J. and Hoffman, J. D., "Scarfed Nozzle Flow Field Calculations," *JANNAF Propulsion Meeting*, CPIA Pub. 340, Vol. 1, May 1981, pp. 213–234.

[10]Romine, G. L. and Noble, J. A., "Closed-Form Model for Three-Dimensional Vacuum Plumes from a Scarfed Nozzle," *AIAA Journal*, Vol. 22, May 1984, pp. 719–720.

[11]Boraas, S., "Analytical Approximation of the Molecular Flow Upstream of the Limiting Streamline," *JANNAF 12th Plume Technology Meeting*, CPIA Pub. 332, Vol. 1, Dec. 1980, pp. 117–138.

[12]Boraas, S., "Backflow Contamination Potential of Rocket Exhausts," *1981 JANNAF Propulsion Meeting*, CPIA Pub. 340, Vol. VI, May 1981, pp. 405–424.

[13]Hill, J. A. F. and Draper, J. P., "Analytical Approximation for the Flow from a Nozzle into a Vacuum," *Journal of Spacecraft and Rockets*, Vol. 10, Oct. 1966, pp. 1552–1559.

[14]Grier, N. T., "Back Flow from Jet Plumes in Vacuum," NASA TN D-4978, Jan. 1969.

[15]Drzewiecki, R. F., Moselle, J. R., and Tsu, C. N., "Characterization of the Peacekeeper Post Boost Vehicle Rocket Exhaust Plumes," *14th JANNAF Plume Technology Meeting*, CPIA Pub. 384, Vol. II, Nov. 1983, pp. 133–156.

[16]Noble, J. A. and Romine, G. L., "MX Stage IV Attitude Control Engine Plume Flowfield Analysis," Martin-Marietta Corp., Marietta, GA, Rept. SE4-116057, Jan. 1981.

[17]Boraas, S., "Development of a Capability of Predicting Performance of and Contamination from Motors with Scarfed Nozzles," Morton Thiokol, Inc./Wasatch Div., Brigham City, UT. Rept. IOM 2814-83-M157, Dec. 1983.